Sensitization of ultra-long-range excited-state electron transfer by energy transfer in a polymerized film

Akitaka Ito, David J. Stewart, Zhen Fang, M. Kyle Brennaman, and Thomas J. Meyer[1]

Department of Chemistry, University of North Carolina at Chapel Hill, Chapel Hill, NC 27599

Contributed by Thomas J. Meyer, August 6, 2012 (sent for review June 20, 2012)

Distance-dependent energy transfer occurs from the Metal-to-Ligand Charge Transfer (MLCT) excited state $Ru(bpy)_3^{2+*}$ to an anthracene-acrylate derivative (Acr-An) incorporated into the polymer network of a semirigid poly(ethyleneglycol)dimethacrylate monolith. Following excitation, $Ru(bpy)_3^{2+*}$ to Acr-An triplet energy transfer occurs followed by long-range, Acr-^{3}An—Acr-An → Acr-An—Acr-^{3}An, energy migration. With methyl viologen dication (MV^{2+}) added as a trap, Acr-^{3}An + MV^{2+} → Acr-An$^+$ + MV^+ electron transfer results in sensitized electron transfer quenching over a distance of approximately 90 Å.

luminescence | time-resolved spectroscopy | polymer matrix

Molecular level electron and energy transfer in rigid and semirigid media are important in applications from imaging to electron transfer in biological membranes (1–4). In photosystem II, the chlorophyll singlet excited state $^1P_{680}{}^*$ is formed by light absorption by an antenna complex followed by highly efficient long-range energy transfer sensitization (5). Oxidative quenching of $^1P_{680}{}^*$ is followed by electron transfer activation of the Oxygen Evolving Complex (OEC) where water is oxidized to oxygen.

Although well understood in solution (6–10), molecular level electron and energy transfer are less well understood in rigid media where diffusion is inhibited and reaction barriers significantly altered (11). There is theoretical (12, 13) and experimental insight into both processes in rigid media with the latter studied largely in low temperature glasses and, to a lesser extent, in plastics and polymeric films (14–17). Important fundamental issues remain to be elucidated along with the possible exploitation of randomly oriented, fixed site geometries in local and long-range electron and energy transfer applications.

Poly(ethyleneglycol)dimethacrylate (PEG-DMA) films and monoliths, Fig. 1*A*, undergo thermal (18–20) or photochemical polymerization under mild conditions (21, 22) to give optically transparent materials with features conformable to the nanoscale. They have proven useful in exploring medium effects on the properties of Metal-to-Ligand Charge Transfer (MLCT) excited states (23). *Here, we report the use of a MLCT excited state in demonstrating sensitized electron transfer induced by ultralong-range energy transfer over a distance of approximately 90 Å.*

Structures relevant to the study are shown in Fig. 1*A*. They include the PEG-DMA derivative with $n = 9$ (PEG-DMA550), the salt $[Ru(bpy)_3](PF_6)_2$, (bpy is 2,2′-bipyridine), and an acrylate derivative of anthracene (Acr-An). The acrylate tail allows the energy and electron transfer active anthracene group to be incorporated into the polymer network as it forms.

Results and Discussion

Fig. 1 *B* and *C* show corrected emission spectra and emission decay profiles, respectively, for $Ru(bpy)_3^{2+*}$ with and without added Acr-An in *poly*-PEG-DMA550. The data provide clear evidence for emission quenching by Acr-An. Emission intensity measurements show that quenching was 55% complete with 300 mM Acr-An in the initial solution. Time-resolved emission measurements revealed rapid (81%) and slow (19%) quenching components (Fig. 1*C*). The rapid component is attributable to instantaneous, nondiffusional quenching at fixed sites in the film and the slower to diffusion of the excited state to Acr-An or of unpolymerized Acr-An to the excited state.

Quenching dynamics were investigated and quenching rate constants (k_q) evaluated by lifetime quenching measurements and the expression, $\tau_0/\tau = \Phi_0/\Phi = 1 + k_q\tau_0[Q]$. In this expression, τ_0 and Φ_0 are the emission lifetime and quantum yields for $Ru(bpy)_3^{2+*}$ in the absence of Acr-An and τ and Φ the same quantities in the presence of Acr-An. [Q] is the concentration of Acr-An in the initial PEG-DMA550 solution. As shown in Fig. 1*D*, plots of τ_0/τ and Φ_0/Φ vs. [Q] for the slow and rapid quenching components, respectively, are linear. Their relative contributions were evaluated at 610 nm from the difference between steady-state and emission-time decay profiles. The fraction of the rapid quenching component increased by decreasing the concentration reaching 98% with 50 mM added Acr-An.

The decrease in lifetime with added Acr-An is due to energy transfer, Eqs. **1** and **2**, with $k_{en,diff}$ and k_{en} the presumed diffusional and fixed site energy transfer rate constants. The lowest-lying MLCT excited state(s) of $Ru(bpy)_3^{2+*}$ are of mixed spin character but largely triplet (24) and energy transfer occurs by exchange energy transfer, the so-called Dexter mechanism (25). Energy transfer is spontaneous with $\Delta G_{en}{}^0 = \Delta G_{ES}(\text{Acr-}^3\text{An}) - \Delta G_{ES}(Ru(bpy)_3^{2+*})$ approximately –0.3 eV. ΔG_{ES} is the free energy of the excited state above the ground state determined by emission spectral fitting, (see *SI Text*, Fig. S1 and Table S1).

From the slopes of the Stern-Volmer plots in Fig. 1*D*, $k_{en} = 2.2 \times 10^6\ M^{-1}\,s^{-1}$ and $k_{en,diff} = 2.9 \times 10^5\ M^{-1}\,s^{-1}$. For the diffusional component this is a decrease of approximately 350 relative to the PEG-DMA550 fluid before polymerization. This rate constant provides a measure of the relatively slow diffusional rates in semirigid *poly*-PEG-DMA.

$$Ru(bpy)_3^{2+*} + \text{Acr-An} \underset{k_{-d}}{\overset{k_d}{\leftrightarrows}} Ru(bpy)_3^{2+*}, \text{Acr-An} \qquad [1A]$$

$$Ru(bpy)_3^{2+*}, \text{Acr-An} \overset{k_{en}}{\rightarrow} Ru(bpy)_3^{2+} + \text{Acr-}^3\text{An} \qquad [1B]$$

Fixed site energy transfer occurs with the quencher sites randomly distributed in the vicinity of the excited state [Eq. **2**]. It is dependent on the average distance separating excited state and quencher, R, with R dependent on the concentration of quencher in the initial solution (26).

$$Ru(bpy)_3^{2+*}\text{—Acr-An} \overset{k_{en}(R)}{\rightarrow} Ru(bpy)_3^{2+}\text{—Acr-}^3\text{An} \qquad [2]$$

$$\left| \xleftrightarrow[R]{} \right|$$

Author contributions: A.I., D.J.S., Z.F., M.K.B., and T.J.M. designed research; A.I. performed research; Z.F. contributed new reagents/analytic tools; A.I. analyzed data; and A.I., D.J.S., Z.F., M.K.B., and T.J.M. wrote the paper.

The authors declare no conflict of interest.

[1]To whom correspondence should be addressed. E-mail: tjmeyer@unc.edu.

This article contains supporting information online at www.pnas.org/lookup/suppl/doi:10.1073/pnas.1213646109/-/DCSupplemental.

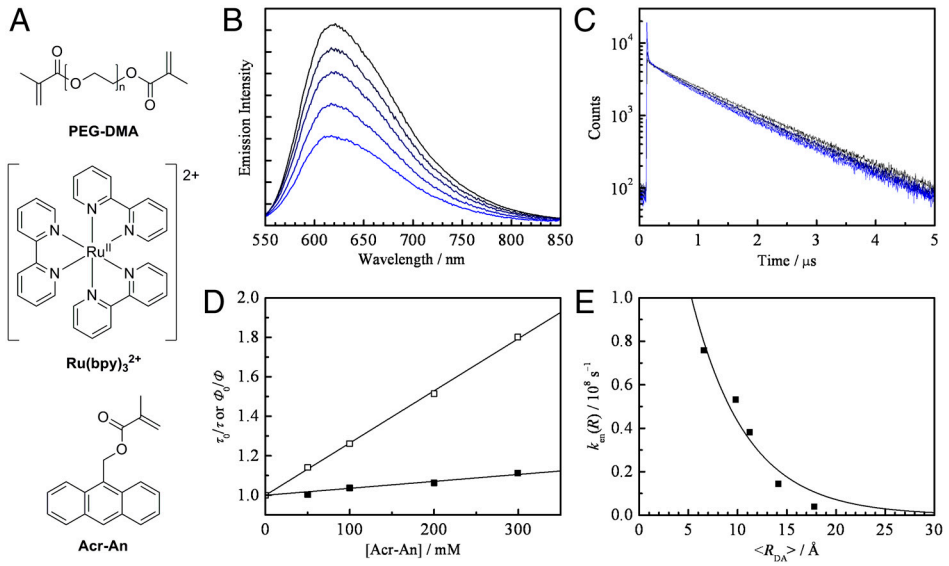

Fig. 1. Structures of PEG-DMA, $Ru(bpy)_3^{2+}$, and Acr-An (*A*). Corrected emission spectra (*B*) and emission decay profiles (*C*) for $Ru(bpy)_3^{2+*}$ in the absence and presence of Acr-An in PEG-DMA550 films: Excitation wavelength = 484 nm. [Acr-An] = 0, 50, 100, 200 and 300 mM (black → blue). Stern-Volmer plots for $Ru(bpy)_3^{2+*}$ quenching by fixed site (open squares) and diffusional quenching (closed squares) by Acr-An in PEG-DMA550 films (*D*). Distance dependence of the rate constant for the fixed site energy transfer component, $k_{en}(R)$, (*E*).

Inokuti and Hirayama evaluated the decay function for Dexter energy transfer by using Eq. **3** (26),

$$I(t) = \exp\left[-\frac{t}{\tau_0} - \gamma^{-3}\frac{c}{c_0}g\left(e^{\gamma}\frac{t}{\tau_0}\right)\right] \quad [3]$$

where c is the acceptor concentration, and c_0 is the critical transfer concentration of the acceptor molecule, defined by $3/(4\pi R_0{}^3)$. The function $g(x)$ in Eq. **3** is defined by

$$g(x) = -x\int_0^1 \exp(-xy)(\ln y)^3 dy \quad [4]$$

Evaluation of k_{en} values was based on the kinetic analysis and Eq. **3** (see *SI Text*, Fig. S2). Fig. 1*E* shows plots of k_{en} as a function of calculated distance between excited state and quencher, $k_{en}(R)$, plotted against the average nearest-neighbor separation distance, $\langle R_{DA}\rangle$. $\langle R_{DA}\rangle$ was calculated from the initial concentration of added quencher, c, by use of Eq. **5** based on the probability distribution of the separation distance R (27).

$$\langle R_{DA}\rangle = \int_0^{\infty} c\exp\left(-\frac{4\pi}{3}cR^3\right)4\pi r^3 dR = 0.55396c^{-\frac{1}{3}} \quad [5]$$

As shown by the plot of $k_{en}(R)$ vs. $\langle R_{DA}\rangle$ in Fig. 1*E*, the exponential distance dependence of k_{en} is consistent with the Dexter mechanism and Eq. **6** (28).

$$k_{en}(R) = k_{R=0}\exp\left(-\frac{2R}{L}\right) = \frac{1}{\tau_0}\exp\left\{\gamma\left(1-\frac{R}{R_0}\right)\right\} \quad [6]$$

In Eq. **6**, $k_{R=0}$ is the hypothetical energy transfer rate constant at $R = 0$, τ_0 is the emission lifetime of excited-state donor with no added quencher; R_0 is the critical intermolecular separation distance at which transfer and spontaneous excited-state decay are equally probable ($k_{en}(R_0) = 1/\tau_0$) and $\gamma = 2R_0/L$. The effective average Bohr radius, $L = 11.2$ Å, was derived from the fit in Fig. 1*E*. By extrapolation of the distance dependence to the approximate close contact distance at 10 Å, $k_{en,0} = 4.3 \times 10^7$ s^{-1}.

Transient absorption measurements were used to confirm that energy transfer had occurred. Fig. 2 shows transient absorption-time decay profiles for PEG-DMA550 films containing $[Ru(bpy)_3](PF_6)_2$ (48 μM), with 50–300 mM added Acr-An, after 460-nm excitation. The monitoring wavelength, 435 nm, is within the ground-excited state absorption bleach for $Ru(bpy)_3^{2+*}$. With no added Acr-An, the negative absorbance at 435 nm decays to the baseline with kinetics characteristic of $Ru(bpy)_3^{2+*}$ decay. With added Acr-An, a new absorption feature appears at 435 nm arising from triplet-triplet absorption by ^{3}An (29). The magnitude of the absorbance change for this feature increases with increasing Acr-An. Its time dependence is qualitatively consistent with the slow and fast components observed in the emission quenching experiments.

The Acr-^{3}An absorption is long-lived with a lifetime inversely dependent on the initial concentration of Acr-An (see *SI Text*, Fig. S3). The limiting lifetime was 5.4 ms by extrapolation. The concentration dependence is due to ^{3}An—^{3}An, triplet-triplet annihilation, Eq. **7** (30, 31). Its appearance demonstrates the existence of a pathway for long-range,

$$\text{Acr-}^3\text{An}^* + \text{Acr-}^3\text{An}^* \rightarrow \text{Acr-}^1\text{An}^* + \text{Acr-An} \quad [7]$$

^{3}An—An → An—^{3}An, energy migration. Triplet-triplet annihilation occurs with $k_{TT} = 4.4 \times 10^3$ M^{-1} s^{-1}, Fig. S3. Related observations have been made for anthracene and anthracene derivatives in acetonitrile by Castellano et al. (32). There was no evidence for upconversion fluorescence from ^{1}An at approximately 380 nm due to self absorption by the ground state.

The combination of energy transfer quenching and long-range ^{3}An—An energy migration creates a basis for ultralong-range, sensitized electron transfer. The potential for the excited-state couple, $An^+ + e^- \rightarrow {}^3An$, is approximately −0.41 V vs. Sodium Saturated Calomel Electrode, SSCE, (−0.17 V vs. NHE) in acetonitrile ($I = 0.1$ M). This estimate is based on the triplet excited-state energy (1.83 eV) (33) and $E^{0\prime} = +1.42$ V vs. SSCE for the $An^+ + e^- \rightarrow An$ couple (34). The potential for the $An^+/{}^3An$ couple is comparable to $E^{0\prime} = -0.44$ V (vs. SSCE in acetonitrile, $I = 0.1$ M) (34) for the methyl viologen, MV^{2+}/MV^+, couple (Fig. 3*A*). The solution values are not relevant to $E^{0\prime}$ values in the films but their relative values point to probable spontaneous electron transfer quenching of ^{3}An by MV^{2+}.

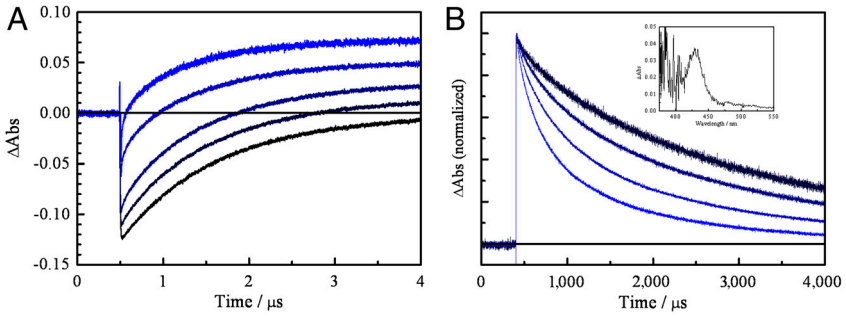

Fig. 2. Transient absorption decay profiles for $Ru(bpy)_3^{2+*}$ with added Acr-An in PEG-DMA550 films observed at 435 nm with short, (*A*), and long-time monitoring, (*B*): [Acr-An] = 0, 50, 100, 200 and 300 mM (black → blue). *Inset*: Transient absorption spectrum of $Ru(bpy)_3^{2+*}$ with 50 mM Acr-An 10 μs after excitation.

Fig. 3 *B* and *C* show transient absorption difference spectra for $Ru(bpy)_3^{2+*}$ with 280 mM added Acr-An with and without 9 mM $MV(PF_6)_2$ added as an electron trap. With all three components added, a new transient absorption feature for MV^+ is evident in the spectrum at $\lambda_{max} = 590$ nm (35) 50 ns after the laser pulse. Also appearing in the spectrum are a diminished bleach for $Ru(bpy)_3^{2+*}$ at 450 nm and the characteristic triplet-triplet Acr-^{3}An absorption feature at 430 nm. Anthracene cation absorptions appear at 430 and 720 nm (36–38), which grow at the expense of Acr-^{3}An. Reduced MV^+ appears even with initial concentrations of $MV(PF_6)_2$ as low as 0.5 mM.

The absorption feature for MV^+ remains in the film for extended periods, >50 μs after excitation. There was no evidence for Acr-^{3}An at 430 nm on this timescale, which is consistent with complete oxidation of the triplet. With 9 mM added MV^{2+} and no added Acr-An, there was no evidence for MV^+ and $Ru(bpy)_3^{2+*}$ excited-state decay was unaffected.

These observations are consistent with long-range sensitized electron transfer by the scheme: Excitation → energy transfer → ^{3}An—An energy migration → electron transfer quenching (Fig. 3*D*). Assuming random distributions of $Ru(bpy)_3^{2+}$ and MV^{2+} in the films, the average internuclear separation distance between $Ru(bpy)_3^{2+*}$ and MV^{2+} can be calculated from $R = (4\pi(c_{Ru(bpy)32+} + c_{MV2+})/3)^{-1/3}$ with the c's as the respective concentrations. With MV^{2+} at 9 mM the average separation distance between $Ru(bpy)_3^{2+*}$ and MV^{2+} is approximately 35 Å. With MV^{2+} at 0.5 mM the distance is >90 Å. The average separation distance between anthracenes is 11 Å at 280 mM added Acr-An. *At this concentration energy migration occurs over a distance of 90 Å requiring at least nine energy migration events*.

The $Ru(bpy)_3^{2+}$-Acr-An-MV^{2+} system is photochromic with back electron transfer, Eq. **8**, occurring with τ approximately 0.3 ms at Acr-An 9 mM. There was no evidence for Acr-An$^+$ oxidation of $Ru(bpy)_3^{2+}$ in the transient data. Slow back electron transfer is predicted to occur because the reaction occurs in the inverted region with ΔG_{bet}^0 approximately −1.9 eV and the initial Acr-An$^+$ hole formed by oxidative quenching of ^{3}An is randomized by An$^+$—An hole migration through the Acr-An crosslinked network.

$$\text{Acr-An}^+ + \text{MV}^+ \rightarrow \text{Acr-An} + \text{MV}^{2+} \qquad \textbf{[8]}$$

The results obtained here describe a new mechanism for long-range sensitization of electron transfer. It is different from sensitized electron transfer in photosystems I and II where an extensive array of coupled light absorbers collect and funnel excitation energy to low-energy chlorophyll light absorbers in the antenna apparatus. In $Ru(bpy)_3^{2+*}$-doped *poly*-PEG-DMA, excitation of single chromophores is coupled to long-range energy transfer through an anthracene network to electron transfer trap sites. We are currently exploring use of this and related phenomena to explore related local and long-range electron and energy transfer events in these semirigid media.

Materials and Methods

Preparation and purification of components are described in the *SI Text*. Samples for photophysical measurements were prepared as free-standing monoliths in 1-cm path length glass cuvettes sealed with rubber septa and

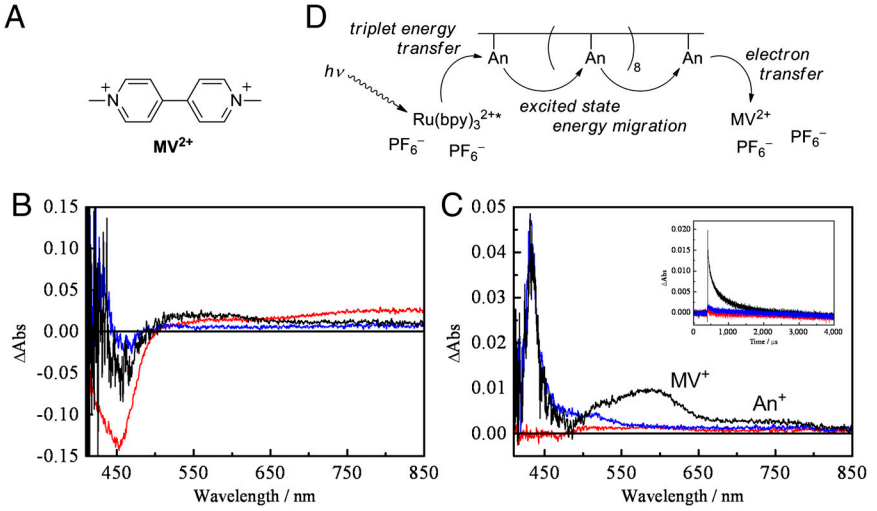

Fig. 3. Structure of MV^{2+} (*A*). Transient absorption spectra following 460-nm excitation of $Ru(bpy)_3^{2+}$ in PEG-DMA 550 with 280 mM Acr-An and 9 mM MV^{2+} (black), 280 mM Acr-An (blue), and 9 mM MV^{2+} (red) at 50 ns (*B*) and 50 μs after excitation (*C*). *Inset*: Transient absorption decay profiles at 600 nm. Schematic illustration of ultra long-range electron transfer (*D*).

evacuated overnight for thorough degassing (23). The concentration of $[Ru(bpy)_3](PF_6)_2$ was 48 or 59 μM. Steady state and transient emission and absorption measurements were conducted at 22 ± 2 °C as described in the *SI Text*.

ACKNOWLEDGMENTS. A.I. (T.J.M.) acknowledges support from the US Department of Energy, Office of Science, Office of Basic Energy Sciences, under Award Number DE-FG02-06ER15788. D.J.S. (T.J.M.) acknowledges support from the National Science Foundation, Award Number NSF 957215. Z.F. (T.J.M., M.K.B.) acknowledges support by the UNC EFRC: Center for Solar Fuels, an Energy Frontier Research Center funded by the US Department of Energy, Office of Science, Office of Basic Energy Sciences under Award Number DE-SC0001011. We acknowledge support for the purchase of instrumentation from the UNC EFRC Center for Solar Fuels, an Energy Frontier Research Center funded by the US Department of Energy, Office of Science, Office of Basic Energy Sciences under Award Number DE-SC0001011, and from UNC SERC ("Solar Energy Research Center Instrumentation Facility" funded by the US Department of Energy, Office of Energy Efficiency and Renewable Energy under Award Number DE-EE0003188).

1. Gaines GL, O'Neil MP, Svec WA, Niemczyk MP, Wasielewski MR (1991) Photoinduced electron transfer in the solid state: Rate vs. free energy dependence in fixed-distance porphyrin-acceptor molecules. *J Am Chem Soc* 113:719–721.
2. Kamat PV, Ford WE (1992) Photochemistry on surfaces. Excited state behavior of ruthenium tris(bathophenanthroline disulfonate) on colloidal alumina-coated silica particles. *Photochem Photobiol* 55:159–163.
3. Jain A, Xu W, Demas JN, DeGraff BA (1998) Binding of luminescent ruthenium(II) molecular probes to vesicles. *Inorg Chem* 37:1876–1879.
4. Komatsu T, Moritake M, Tsuchida E (2003) Molecular energy and electron transfer assemblies made of self-organized lipid-porphyrin bilayer vesicles. *Chem Eur J* 9:4626–4633.
5. Kühlbrandt W (1994) Structure and function of the plant light-harvesting complex, LHC-II. *Curr Opin Struct Biol* 4:519–528.
6. Birks JB (1970) *Photophysics of Aromatic Hydrocarbons* (Wiley-Interscience, London).
7. Bock CR, et al. (1979) Estimation of excited-state redox potentials by electron-transfer quenching. Application of electron-transfer theory to excited-state redox processes. *J Am Chem Soc* 101:4815–4824.
8. Meyer TJ (1983) Excited-state electron transfer. *Prog Inorg Chem* 30:389–440.
9. Kavarnos GJ, Turro NJ (1986) Photosensitization by reversible electron transfer: Theories, experimental evidence, and examples. *Chem Rev* 86:401–449.
10. Kitamura N, Kim H-B, Okano S, Tazuke S (1989) Photoinduced electron-transfer reactions of Ruthenium(II) complexes. 1. Reductive quenching of excited $Ru(bpy)_3^{2+}$ by aromatic amines. *J Phys Chem* 93:5750–5756.
11. Beitz JV, Miller JR (1979) Exothermic rate restrictions on electron transfer in a rigid medium. *J Chem Phys* 71:4579–4595.
12. Marcus RA (1990) Theory of charge-transfer spectra in frozen media. *J Phys Chem* 94:4963–4966.
13. Chen P, Meyer TJ (1996) Electron transfer in frozen media. *Inorg Chem* 35:5520–5524.
14. Guarr T, McGuire ME, McLendon G (1985) Long range photoinduced electron transfer in a rigid polymer. *J Am Chem Soc* 107:5104–5111.
15. Dick LA, et al. (1998) Cryogenic electron tunneling within mixed-metal hemoglobin hybrids: Protein glassing and electron-transfer energetics. *J Am Chem Soc* 120:11401–11407.
16. Gray HB, Winkler JR (2005) Long-range electron transfer. *Proc Natl Acad Sci USA* 102:3534–3539.
17. Wenger OS, Leigh BS, Villahermosa RM, Gray HB, Winkler JR (2005) Electron tunneling through organic molecules in frozen glasses. *Science* 307:99–102.
18. He SL, Yaszemski MJ, Yasko AW, Engel PS, Mikos AG (2000) Injectable biodegradable polymer composites based on poly(propylene fumarate) crosslinked with poly(ethylene glycol)-dimethacrylate. *Biomaterials* 21:2389–2394.
19. Liu J, Teo WK, Chew CH, Gan LM (2000) Nanofiltration membranes prepared by direct microemulsion copolymerization using poly(ethylene oxide) macromonomer as a polymerizable surfactant. *J Appl Polym Sci* 77:2785–2794.
20. Fleming CN, Brennaman MK, Papanikolas JM, Meyer TJ (2009) Efficient, long-range energy migration in Ru(II) polypyridyl derivatized polystyrenes in rigid media. Antennae for artificial photosynthesis. *Dalton Trans* 3903–3910.
21. Kim P, et al. (2005) Fabrication of nanostructures of Pplyethylene glycol for applications to protein adsorption and cell adhesion. *Nanotechnology* 16:2420–2426.
22. Hu Z, et al. (2008) Optically transparent, amphiphilic networks based on blends of perfluoropolyethers and poly(ethylene glycol). *J Am Chem Soc* 130:14244–14252.
23. Knight TE, et al. (2011) Influence of the fluid-to-film transition on photophysical properties of MLCT excited states in a polymerizable dimethacrylate fluid. *J Phys Chem B* 115:64–70.
24. Kober EM, Meyer TJ (1982) Concerning the absorption spectra of the ions $M(bpy)_3^{2+}$ (M = Fe, Ru, Os, bpy = 2, 2′-bipyridine). *Inorg Chem* 21:3967–3977.
25. Dexter DL (1953) A theory of sensitized luminescence in solids. *J Chem Phys* 21:836–850.
26. Inokuti M, Hirayama F (1965) Influence of energy transfer by the exchange mechanism on donor luminescence. *J Chem Phys* 43:1978–1989.
27. Minn FL, Filipescu N (1970) Nearest-neighbour model for transfer of electronic excitation energy. *J Chem Soc A* 1016–1020.
28. Ito A, Meyer TJ (2012) The Golden Rule. Application for fun and profit in electron transfer, energy transfer, and excited-state decay. *Phys Chem Chem Phys*, in press.
29. Dempster DN, Morrow T, Quinn MF (1973) Extinction coefficients for triplet-triplet absorption in ethanol solutions of anthracene, naphthalene, 2,5-diphenyloxazole, 7-diethylamino-4-methyl coumarin and 4-methyl-7-amino-carbostyril. *J Photochem* 2:329–341.
30. Livingston R, Tanner DW (1958) The triplet state of anthracene in liquid solutions. *Trans Faraday Soc* 54:765–771.
31. Lower SK, El-Sayed MA (1966) The triplet state and molecular electronic processes in organic molecules. *Chem Rev* 66:199–241.
32. Islangulov RR, Kozlov DV, Castellano FN (2005) Low power upconversion using MLCT sensitizers. *Chem Commun* 30:3776–3778.
33. Murtaza Z, et al. (1994) Energy transfer in the inverted region: Calculation of relative rate constants by emission spectral fitting. *J Phys Chem* 98:10504–10513.
34. Younathan JN, Jones WE, Meyer TJ (1991) Energy- and electron-transfer shuttling by a soluble, bifunctional redox polymer. *J Phys Chem* 95:488–492.
35. Watanabe T, Honda K (1982) Measurement of the extinction coefficient of the methyl viologen cation radical and the efficiency of its formation by semiconductor photocatalysis. *J Phys Chem* 86:2617–2619.
36. Yamamoto Y, Ma X-H, Hayashi K (1987) Pulse radiolysis study of the formation of aromatic radical cations enhanced by diphenyliodonium salts. *J Phys Chem* 91:5343–5347.
37. Fujita M, Fukuzumi S (1993) Electron-transfer oxidation of 9-alkylanthracenes and the decay kinetics of radical cations in acetonitrile. *Chem Lett* 22:1911–1914.
38. Naqvi KR, Melø TB (2006) Reduction of tetranitromethane by electronically excited aromatics in acetonitrile: Spectra and molar absorption coefficients of radical cations of anthracene, phenanthrene and pyrene. *Chem Phys Lett* 428:83–87.